

## Controlled Synthesis of 2-D and 3-D Dendritic Platinum Nanostructures

Yujiang Song,<sup>†,‡</sup> Yi Yang,<sup>†,‡</sup> Craig J. Medforth,<sup>†</sup> Eulalia Pereira,<sup>†,§</sup> Anup K. Singh,<sup>†</sup>  
Huifang Xu,<sup>‡</sup> Yingbing Jiang,<sup>‡</sup> C. Jeffrey Brinker,<sup>†,‡</sup> Frank van Swol,<sup>†,‡</sup> and  
John A. Shelnutt<sup>\*,†,‡</sup>

*Contribution from the Advanced Materials Laboratory, Sandia National Laboratories, Albuquerque, New Mexico 87106, Departments of Chemistry, Chemical and Nuclear Engineering, and Earth and Planetary Sciences, University of New Mexico, Albuquerque, New Mexico 87131, CEQUP/Departamento de Química, Faculdade de Ciências, Universidade do Porto, Porto, Portugal, and Department of Chemistry, University of Georgia, Athens, Georgia 30602*

Received July 22, 2003; E-mail: jasheln@unm.edu

**Abstract:** Seeding and autocatalytic reduction of platinum salts in aqueous surfactant solution using ascorbic acid as the reductant leads to remarkable dendritic metal nanostructures. In micellar surfactant solutions, spherical dendritic metal nanostructures are obtained, and the smallest of these nanodendrites resemble assemblies of joined nanoparticles and the nanodendrites are single crystals. With liposomes as the template, dendritic platinum sheets in the form of thin circular disks or solid foamlike nanomaterials can be made. Synthetic control over the morphology of these nanodendrites, nanosheets, and nanostructured foams is realized by using a tin-porphyrin photocatalyst to conveniently and effectively produce a large initial population of catalytic growth centers. The concentration of seed particles determines the ultimate average size and uniformity of these novel two- and three-dimensional platinum nanostructures.

### Introduction

Metal nanostructures are of considerable interest because of their importance in catalysis,<sup>1</sup> photochemistry,<sup>2</sup> sensors,<sup>3</sup> tagging,<sup>4</sup> and optical,<sup>5</sup> electronic,<sup>5</sup> and magnetic devices.<sup>3,6</sup> Metal nanostructures have been synthesized in many forms, ranging from conventional metal colloids<sup>3,5</sup> to modern near-monodispersed nanoclusters,<sup>7–16</sup> shape-controlled nanocrystals,<sup>17–21</sup> and

other nanostructures such as wires<sup>22,23</sup> and sheets.<sup>24</sup> Nanostructured platinum is of particular interest for many applications, including catalysis,<sup>2,17,25</sup> sensors,<sup>26</sup> and other devices.<sup>25,27–29</sup> While a few platinum nanostructures have been reported, including nanoparticles,<sup>17,18</sup> nanowires,<sup>22,23</sup> nanosheets,<sup>24</sup> and others,<sup>30–33</sup> the synthesis of additional types of nanostructures is highly desirable and potentially technologically important.

New methods for the synthesis of metal nanostructures are important for providing the reproducibility and control over

<sup>†</sup> Sandia National Laboratories.

<sup>‡</sup> University of New Mexico.

<sup>§</sup> Universidade do Porto.

<sup>‡</sup> University of Georgia.

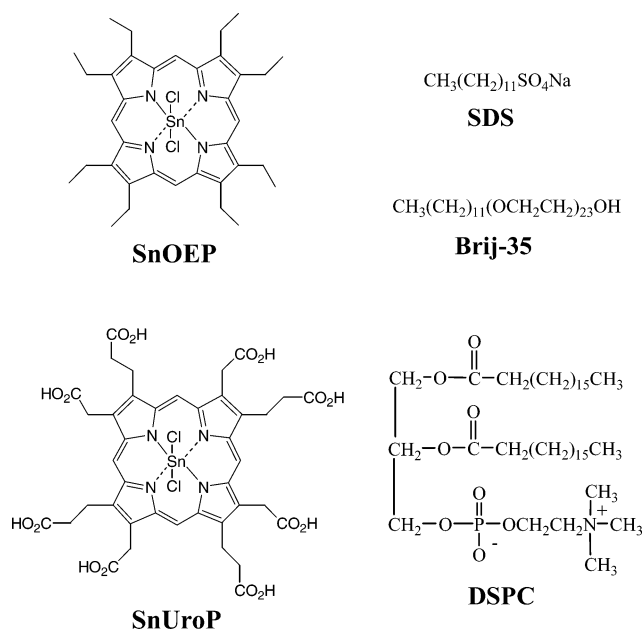
- (1) Hirai, H.; Wakabayashi, H.; Komiyama, M. *Chem. Lett.* **1983**, 1047–1050.
- (2) Brugger, P. A.; Cuendet, P.; Gratzel, M. *J. Am. Chem. Soc.* **1981**, *103*, 2923–2927.
- (3) Thomas, J. M. *Pure Appl. Chem.* **1988**, *60*, 1517–1518.
- (4) Mulvaney, S. P.; Musick, M. D.; Keating, C. D.; Natan, M. J. *Langmuir* **2003**, *19*, 4784–4790.
- (5) Schon, G.; Simon, U. *Colloid Polym. Sci.* **1995**, *273*, 202–218.
- (6) Skomski, R. *J. Phys.: Condens. Matter* **2003**, *15*, R841–R896.
- (7) Turkevich, J. *Discuss. Faraday Soc.* **1951**, *11*, 55.
- (8) Turkevich, J.; Kim, G. *Science* **1970**, *169*, 873.
- (9) Belloni, J. *Curr. Opin. Colloid Interface Sci.* **1996**, *1*, 184–196.
- (10) Henglein, A. *Chem. Rev.* **1989**, *89*, 1861–1873.
- (11) Roucoux, A.; Schultz, J.; Patin, H. *Chem. Rev.* **2002**, *102*, 3757–3778.
- (12) Finke, R. G., In *Metal Nanoparticles: Synthesis, Characterization, and Applications*; Feldheim, D. L., Foss, C. A., Jr., Eds.; Marcel Dekker: New York, 2002; pp 17–54.
- (13) Watzky, M. A.; Finke, R. G. *J. Am. Chem. Soc.* **1997**, *119*, 10382–10400.
- (14) Watzky, M. A.; Finke, R. G. *Chem. Mater.* **1997**, *9*, 3083–3095.
- (15) Widegren, J. A.; Aiken, J. D., III; Ozkar, S.; Finke, R. G. *Chem. Mater.* **2001**, *13*, 312–324.
- (16) Yu, H.; Gibbons, P. C.; Kelton, K. F.; Buhro, W. E. *J. Am. Chem. Soc.* **2001**, *123*, 9198–9199.
- (17) Ahmadi, T. S.; Wang, Z. L.; Green, T. C.; Henglein, A.; El-Sayed, M. A. *Science* **1996**, *272*, 1924–1926.
- (18) Ahmadi, T. S.; Wang, Z. L.; Henglein, A.; El-Sayed, M. A. *Chem. Mater.* **1996**, *8*, 1161–1163.
- (19) Jana, N. R.; Gearheart, L.; Murphy, C. J. *Adv. Mater.* **2001**, *13*, 1389–1393.
- (20) Jana, N. R.; Wang, Z. L.; Sau, T. K.; Pal, T. *Curr. Sci.* **2000**, *79*, 1367–1370.
- (21) Teranishi, T.; Kurita, R.; Miyake, M. *J. Inorg. Organomet. Polym.* **2000**, *10*, 145–156.
- (22) Melosh, N. A.; Doukai, A.; Diana, F.; Gerardot, B.; Badolato, A.; Petroff, P. M.; Heath, J. R. *Science* **2003**, *300*, 112–115.
- (23) Han, Y. J.; Kim, J. M.; Stucky, G. D. *Chem. Mater.* **2000**, *12*, 2068–2069.
- (24) Shirai, M.; Igeta, K.; Arai, M. *Chem. Commun.* **2000**, 623–624.
- (25) Chen, C. W.; Serizawa, T.; Akashi, M. *Chem. Mater.* **1999**, *11*, 1381–1389.
- (26) Matko, I.; Gaidi, M.; Hazemann, J. L.; Chenevier, B.; Labeau, M. *Sensors Actuators-Chem.* **1999**, *59*, 210–215.
- (27) Carpenter, E. E.; Sims, J. A.; Wienmann, J. A.; Zhou, W. L.; O'Connor, C. J. *J. Appl. Phys.* **2000**, *87*, 5615–5617.
- (28) De, S.; Pal, A.; Pal, T. *Langmuir* **2000**, *16*, 6855–6861.
- (29) Joo, S. H.; Choi, S. J.; Oh, I.; Kwak, J.; Liu, Z.; Terasaki, O.; Ryoo, R. *Nature* **2001**, *412*, 169–172.
- (30) Gómez, M.; Philippot, K.; Collière, V.; Lecante, P.; Muller, G.; Chaudret, B. *New J. Chem.* **2003**, *27*, 114–120.
- (31) Shin, H. J.; Ko, C. H.; Ryoo, R. *J. Mater. Chem.* **2001**, *11*, 260–261.
- (32) Wakayama, E. H.; Fukushima, Y. *Chem. Commun.* **1999**, 391–392.
- (33) Komatsu, R.; Uda, S. *Mater. Res. Bull.* **1998**, *33*, 433–440.

properties required for advanced technological applications. A recognized goal of these new synthetic approaches is to achieve control over the composition, size, surface species, solubility, stability, isolability, and other functional properties of the nanostructures.<sup>11</sup> For example, a mechanism consisting of nanoparticle seeding followed by fast autocatalytic surface growth gives nearly monodisperse nanoclusters for a variety of metals.<sup>7–10,16,19,20,34–36</sup> Thus, nearly monodisperse nanoclusters of iridium have been attained by H<sub>2</sub> reduction of iridium salts.<sup>12–15</sup> Copper nanoparticles of controlled shape and size were prepared in solution without any capping agent or template by seeding and subsequent reduction of copper ions by ascorbate at the particle surfaces.<sup>20</sup> Particle size was selected by varying the ratio of copper seed particles to copper ion concentration. Shape-controlled platinum nanocrystals<sup>17,21</sup> have been synthesized using a capping polymer material, giving mixtures of tetrahedral, cubic, irregular-prismatic, icosahedral, and cubo-octahedral nanoparticles.<sup>17</sup> The shapes produced are determined by interfacially directed control over the relative growth rates of different crystalline faces. Nanosheets have been produced by reduction of platinum chloride intercalation compounds confined between graphite layers.<sup>24,37</sup>

Herein, we describe a method of synthesis that leads to novel types of fractal-shaped platinum nanostructures of controlled sizes. This synthetic method is based on a seeding and fast autocatalytic growth approach in which an aqueous solution of platinum salts is reduced by ascorbic acid in the presence of surfactant. The seeding/autocatalytic approach employed by us in the present study produces nanodendrites, which grow by interfacially directed autocatalytic reduction of platinum onto the platinum nanoparticle seeds. To our knowledge, metallic platinum nanodendrites have not been made previously by autocatalytic growth or by any similar approach. (Platinum dendrites of considerably different morphology have been grown from lithium tetraborate melts by the Czochralski method.<sup>33</sup> The present approach is different from the conventional growth of dendrites by diffusion-limited crystallization of metals or by the Czochralski method.)

In the case of micellar solutions, the new synthesis yields three-dimensional metallic platinum nanodendrites of diameters ranging from 6 to 200 nm. When large liposomes are used, dendritic disklike nanosheets or dendritic sheets in the form of solid foamlike nanomaterials are produced depending on the experimental conditions, indicating a templating effect of the surfactant assembly. Control over the size of these dendritic nanostructures is conveniently realized by using a tin-porphyrin photocatalyst to rapidly generate an initial population of growth centers. In the case of the three-dimensional nanodendrites, this photocatalytic seeding approach can be used to produce nanostructures with average sizes in the range 10–50 nm and narrow size distributions. The effects of light exposure and photocatalyst concentration on the size of the nanodendrites are evaluated in detail, and these studies are crucial in verifying the proposed seeding/autocatalytic growth mechanism. Finally, it is demonstrated that the small three-dimensional platinum nanodendrites

**Chart 1.** Structures of the Porphyrin Photocatalysts and Surfactants.



obtained by the photocatalytic synthetic method are functional catalytic/photocatalytic units capable of H<sub>2</sub> evolution from water.

#### Materials and Methods.

**Materials.** Potassium tetrachloroplatinate(II) (K<sub>2</sub>PtCl<sub>4</sub>; 99.99%), L-ascorbic acid (99+%), sodium dodecyl sulfate (SDS), polyoxyethylene (23) lauryl ether (Brij-35), 1,2-dioctadecanoyl-*sn*-glycero-3-phosphocholine (DSPC, 99%), and cholesterol (99+%) were of the highest purity available and were used as received from Sigma-Aldrich (St. Louis, MO). Sn(IV) octaethylporphyrin dichloride (SnOEP) and Sn(IV) uroporphyrin I (SnUroP) were obtained from Porphyrin Products (Logan, UT) and used without further purification. The chemical structures of the surfactants and porphyrin photocatalysts are shown in Chart 1. Sn and Ni tetra(*N*-methylpyridinium)porphyrin (T(N-Me-Py)P) were also obtained from Porphyrin Products and used as obtained (structures not shown). All aqueous solutions were prepared with ultrapure water from a Barnstead Nanopure water system (Chesterland, OH).

**Preparation of Reactant and Surfactant Solutions.** Platinum(II) solution was prepared by dissolving K<sub>2</sub>PtCl<sub>4</sub> in water under ambient condition and was aged at least 24 h before use. Aging the platinum solution disproportionates the complex into an equilibrium mixture of 42% Pt(H<sub>2</sub>O)<sub>2</sub>Cl<sub>2</sub>, 53% Pt(H<sub>2</sub>O)Cl<sub>3</sub><sup>-</sup>, and 5% PtCl<sub>4</sub><sup>2-</sup>.<sup>38</sup> SDS (80 mM) or Brij-35 (1 mM) micellar stock solutions were prepared by dissolving SDS or Brij-35 in water with mild sonication. The porphyrin-saturated surfactant solutions were prepared by dissolving SnOEP in these SDS or Brij-35 solutions using mild sonication. Undissolved suspended SnOEP was filtered off using a 200 nm pore filter (VWR Scientific Products, West Chester, PA), and this porphyrin stock solution (10–175 μM in SnOEP and 80 mM in SDS or 1 mM in Brij-35) was diluted to the desired concentration for use in the reaction. Solutions of nickel(II) and tin(IV) T(N-Me-Py)P were prepared in a similar manner. The ascorbic acid solution was freshly prepared because of its gradual oxidation in air; the oxidation is evidenced by the decrease in the ascorbic acid UV absorption bands (see Figure S1 of the Supporting Information and the discussion below).

Multilamellar vesicles with different sizes were prepared by intense sonication of an 8 mM DSPC aqueous solution containing ascorbic

(34) Jana, N. R.; Gearheart, L.; Murphy, C. J. *Chem. Mater.* **2001**, *13*, 2313–2322.

(35) Jana, N. R.; Pal, T. *Curr. Sci.* **1998**, *75*, 145–149.

(36) Sau, T. K.; Pal, A.; Jana, N. R.; Wang, Z. L.; Pal, T. *J. Nanopart. Res.* **2001**, *3*, 257–261.

(37) Shirai, M.; Igeta, K.; Arai, M. *J. Phys. Chem. B* **2001**, *105*, 7211–7215.

(38) Ciacchi, L. C.; Pompe, W.; De Vita, A. *J. Am. Chem. Soc.* **2001**, *123*, 7371–7380.

acid (150 mM) using a Misonix ultrasonic processor XL (Farmingdale, NY). Unilamellar liposomes with a composition of 1:1 DSPC/cholesterol mole ratio were prepared by an extrusion procedure. Stock solutions typically at a concentration of 10 mg/mL of lipids were prepared in 9:1 chloroform/methanol (v/v). Mixtures of various lipids amounting to 10  $\mu\text{mol}$  total were added to a round-bottomed flask. The flask was connected to a rotary evaporator and dried at 60 °C for 1.5 h to form a thin lipid film on the inside wall of the flask. The dried lipid layer was then hydrated in 3 mL of filtered and degassed water or aqueous 150 mM ascorbic acid for 1 h at 65 °C to form multilamellar liposomes. The multilamellar liposomes were sonicated briefly in a bath sonicator to reduce the average size of liposomes and then extruded through a 100 nm pore polycarbonate membrane in a pneumatic liposome extruder (Liposfast, Avestin, Ontario, Canada). Liposomes were extruded 31 times to ensure uniform size distribution. The resulting unilamellar liposome suspension was centrifuged for 20 min at 3000g to remove residual multilamellar liposomes and aggregated lipids. Liposome solutions in water and in aqueous ascorbic acid were prepared both with and without 333 nM SnOEP.

**Characterization of the Surfactant Assemblies.** The liposomes were characterized by determining the hydrodynamic diameter of the liposome in solution, estimated using a quasi-elastic light scattering (QELS) apparatus (Brookhaven Instruments, Holtsville, NY, or Beckman-Coulter, Hialeach, FL). The liposomal solutions (50  $\mu\text{L}$ ) were diluted in 1.5 mL of freshly filtered solution in a polypropylene cuvette and placed in the QELS apparatus. The measurement was performed at 90° scattering angle, and the QELS data were analyzed using the constrained regularization (CONTIN) method to obtain a mean diameter and distribution. The hydrodynamic diameters obtained for the unilamellar liposomes from the dynamic light scattering measurements were 161.6 nm for the porphyrin-containing liposomes and 175.1 nm for the control porphyrin-free liposomes. Zeta potentials of the liposome solutions were measured by electrophoretic light scattering. Liposomes were diluted in a 10 mM KCl solution for the measurement of the zeta potentials; the zeta potential was  $-1.55 \pm 0.65$  mV.

The size of the multilamellar DSPC vesicles in solutions was determined by dynamic light scattering measurements using a Beckman Coulter N5 submicron particle size analyzer with a 25 mW He-Ne laser (632.8 nm). The scattering angle was 90°, and the intensity autocorrelation functions were fitted using PCS control software (Version 2.02) to derive hydrodynamic diameters. Average vesicle diameters produced ranged from 57 to 400 nm by QELS measurements depending on the sonication times.

**Synthesis of Platinum Nanostructures.** In a typical synthesis using micellar solutions, 0.125 mL of the aqueous stock solution containing SDS (80 mM) or Brij-35 (1.0 mM) micelles was added to a glass reaction vessel. To this solution was added SnOEP to the desired concentration (0–35  $\mu\text{M}$ ) by making microliter-scale additions from the porphyrin-surfactant stock solutions. Then, 0.25 mL of the Pt salt solution (20 mM) and 0.25 mL of an ascorbic acid solution (150 mM; containing the surfactant at the same concentrations given above) were added stepwise to the reaction vessel. The pH of this reaction solution was 3.0. The reaction vessel containing the solution was irradiated with incandescent light (800 nmol  $\text{cm}^{-2}$   $\text{s}^{-1}$ ) for 30 min. The light intensity was measured with a Hansatech Instruments (Norfolk, England) Quantitherm light meter thermometer; intensities range from ambient room light (0.5–2.0 nmol  $\text{cm}^{-2}$   $\text{s}^{-1}$ ) to intense incandescent irradiation from a projector (800 nmol  $\text{cm}^{-2}$   $\text{s}^{-1}$ ). At the highest intensities, some heating from the light source occurred, but controlled temperature studies showed that the heating had negligible effect on the platinum nanostructure product. The color of the reaction solution changed within 10 min from transparent light brownish-yellow (from the Pt complex) to brownish-gray to opaque black.

In a typical synthesis of the liposome-templated nanostructures, similar volumes of the aqueous solutions containing DSPC/cholesterol liposomes, aged Pt complex (8 mM), and ascorbic acid (60 mM) were

mixed and irradiated with incandescent light for 30 min. For some of the solutions the DSPC liposomes also contained SnOEP. The reaction solution turned black during irradiation at a slower rate than the micellar reactions, with the reaction rate depending on the intensity of irradiation and size of the surfactant assembly.

**Characterization of Platinum Nanomaterials.** Transmission electron microscopy (TEM, 200 keV JEOL 2010), high-resolution TEM (HRTEM), high-angle annular dark-field (HAADF) scanning TEM (200 keV JEOL 2010F), selected-area electron diffraction, and energy-dispersive X-ray spectroscopy were performed on the nanostructures. The samples for TEM analysis were prepared by adding drops of colloidal solutions onto standard holey carbon-coated copper grids. The excess solvent was wicked away with a filter paper, and the grids were dried in air.

Dynamic light scattering measurements to determine the size of the platinum nanostructures in solutions were performed with a Beckman Coulter N4+ or N5 submicron particle size analyzer. The scattering angle was 90°, and the intensity autocorrelation functions were fitted using PCS control software to derive hydrodynamic diameters. UV-visible absorption spectra were obtained with a HP8452A diode array spectrophotometer (Colorado Springs, CO) using a 1 mm path length quartz cell.

**Hydrogen Evolution Measurements.** The solution for the H<sub>2</sub> evolution reaction contained ascorbic acid (60 or 200 mM) and the highly diluted product of the photocatalyzed reactions producing platinum nanodendrites (6.5 or 65  $\mu\text{M}$  in Pt). (The nanodendrites produced in these reactions are similar to those shown in the TEM image of Figure 4b.) SnUroP was also added to a final concentration of 80  $\mu\text{M}$  for improved light-harvesting function. The volume of the liquid sample in the vessel was 2.5 mL. The reaction vessel consisted of a 6 in. round-bottom Pyrex tube 0.75 in. in diameter that was sealed with a rubber septum. The reaction vessel was irradiated with a tungsten light source (800 nmol  $\text{cm}^{-2}$   $\text{s}^{-1}$  at the vessel), and samples were removed periodically for analysis. All reactions were run under an argon atmosphere.

Gas chromatography (GC) (HP 5890 Series II instrument controlled by HP ChemStation, version A0701 software, Gaithersburg, MD) was used to quantify the H<sub>2</sub> gas produced photocatalytically by the platinum nanostructures. The GC instrument was calibrated immediately before the measurements by adding known amounts of H<sub>2</sub> to a control reaction mixture. All gas samples (typically 100  $\mu\text{L}$ ) were extracted from the void volume of reaction vessel and were manually injected with a syringe onto a 100/120 Carbosieve SII column (10 feet length, 1/8 in. width) and carried by argon at a constant flow rate of 100  $\text{cm}^3$   $\text{min}^{-1}$  to a thermal conductivity detector operating at 110 °C. The retention time for hydrogen was about 1.4 min.

## Results and Discussion.

**Nanostructures Obtained by Ascorbic Acid Reduction of Platinum in the Presence of Surfactant.** In the absence of surfactant, the reduction of platinum salts by ascorbic acid occurs in minutes and results in macroscopic pieces of platinum metal that settle out within 10 min. However, reduction in the presence of large unilamellar liposomes has a dramatic effect on the morphology of the platinum obtained from the reaction. When 160 nm diameter unilamellar distearoyl-phosphatidylcholine (DSPC; see Chart 1) liposomes are used in the reaction, TEM images of the product exhibit the two-dimensional circular nanostructures shown in Figure 1. Both electron diffraction (inset of Figure 1) and energy-dispersive X-ray spectra (Figure S2a) of dried samples confirm that the nanostructures observed are composed of platinum. The thickness of the interior portion of the nanosheets can be estimated from the platinum thickness at the particle-like tips of the circular nanosheets (~3 nm),

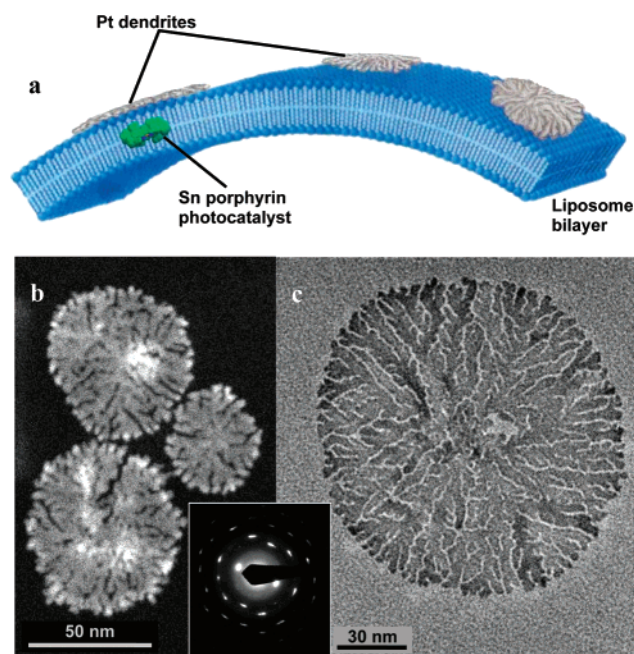


**Figure 1.** Dendritic platinum circular nanosheets templated by liposomes. (a) Illustration of the growth of Pt nanosheets on the liposomal surface; other possible growth mechanisms are discussed in the text. (b) HAADF scanning TEM image of three platinum circular nanosheets grown on 160 nm diameter DSPC liposomes. (c) TEM image of a large dendritic Pt nanosheet made using DSPC liposomes and (inset) its electron diffraction pattern. The surfactant assemblies cannot be seen in the TEM images because of the lack of contrast with the much denser Pt and the interference from the carbon film of the TEM grid.

suggesting the sheets are approximately 2 nm thick.<sup>39</sup> Scanning TEM using a high-angle annular dark-field (HAADF) detector allows one to image nanostructures as small as single atoms using the electrons scattered to high angle.<sup>40</sup> HAADF has many advantages,<sup>41</sup> but in this work we take advantage of HAADF to provide the  $z$ -density projection of the nanostructures for profile imaging. Density profiles (not shown) obtained from the scanning TEM HAADF images (Figure 1b) show that the arms of the dendrites generally have a uniform thickness, except at the tips. The platinum nanosheets are obtained in varying diameters, but nanodendrites of more uniform diameter can be obtained by initially seeding the reaction with 3 nm platinum particles or by in situ photocatalytic generation of Pt seed particles as described below.

Figures 1b and 1c show that these two-dimensional nanosheets are unmistakably dendritic. The fractal dimensions of these nanosheets were obtained by analysis of the TEM images of 10 of the two-dimensional dendrites such as that shown in Figure 1 using the programs Fractal Dimension Version 1.1 (<http://polymer.bu.edu/ogaf/html/software.htm>) and Fractal Dimension Calculator (<http://astronomy.swin.edu.au/~pbourke/fractals/fracdim/>). The average fractal dimension is  $1.73 \pm 0.08$  when analyzed using the box-counting method with the box size varied over two decades. This value of the fractal dimension is typical of computer simulations of two-dimensional aggregation when

only single particles are allowed to diffuse by Brownian motion (1.7) and considerably different from cases in which particle clusters can diffuse (1.4) or particle motion is linear.<sup>42,43</sup> In the present case, metal atoms are not thought to diffuse, but there is a diffusion-limited process in which ascorbic acid and Pt complex diffuse to the surface of the growing metal dendrite and react (see discussion below).

The circular nanosheets are most likely templated by the liposomal surface, possibly on the surface as illustrated in Figure 1a or within the bilayer. Another intriguing possibility is that the nanosheet starts to grow on a liposome, then sticks to another liposome and continues to grow at the interface between the two liposomes. In this case, reactants would be available for growth only by diffusion into the interfacial region between the two liposomes, and thus reactants would be preferentially available to the tips of the dendrite.

Large ( $\sim 100$ – $500$  nm) multilamellar vesicles of DSPC also serve as templates for producing the Pt nanosheets. Interestingly, changing the size of these vesicles at a constant DSPC concentration by sonication alters the morphology of the platinum nanostructure obtained from the subsequent reaction. For example, with small vesicles (57 nm) prepared by intense sonication of the large multilayer vesicles, the reaction gives nanoparticle groupings and only a few small poorly formed dendritic nanosheets. This result suggests that it is the curvature of the surfactant assembly that determines the dimensionality of the dendrites. Apparently, the surface curvature of the small vesicles is too great to support Pt growth in sheets, consistent with a templating role for the large liposomes as discussed in more detail below.

The detailed structure of the circular nanosheets is revealed by high-resolution TEM images and electron diffraction. The electron diffraction pattern of the nanosheet in Figure 1c is shown in the inset; it indicates that metal growth occurs in essentially the same crystallographic orientation throughout the dendrite. Crystal bending can be seen directly in the lattice fringing of high-resolution images (Figure S3 of the Supporting Information), thus crystal bending and an occasional low-angle grain boundary account for the elongated points of the electron diffraction pattern in the inset in Figure 1. The directions of the crystallographic axes vary by up to  $10^\circ$  based on the elongation of the points in the diffraction pattern.

The two-dimensional platinum nanostructures take on a different form when they are prepared under different conditions. When the liposomes are prepared in water rather than an ascorbic acid solution and then added to an ascorbic acid solution (60 mM) for the platinum reduction reaction, the platinum produced appears as balls of dendritic nanosheets (see Figure 2). These porous wads of nanosheets are not observed when the liposomes are prepared in ascorbic acid; instead, the reaction gives mostly the circular nanosheets shown in Figure 1. For the liposomes prepared in water, differences in chemical potential between the water on the inside of the liposome and the solution of ascorbic acid and Pt salt on the outside of the liposome likely disrupt the normal liposomal structure and cause aggregation, giving rise to the foamlike Pt material observed in the TEM images.

(39) We are aware of only one other clear example of the preparation of platinum nanosheets. Shirai et al. (ref 24) have obtained platinum sheets of a thickness of 2–3 nm by confined growth between layers of graphite by hydrogen reduction of platinum chloride intercalation compounds. These nanosheets contain hexagonal holes in an uncontrolled pattern and, in contrast with those observed in the present work, are not dendritic in nature.

(40) Crewe, A. V. *Chem. Scr.* **1979**, *14*, 17–20.

(41) Wang, Z. L. *Adv. Mater.* **2003**, *13*, 1497–1514.

(42) Witten, T. A.; Sander, L. M. *Phys. Rev. Lett.* **1981**, *47*, 1400–1403.

(43) Hurd, A. J. In *Physics of Complex and Supermolecular Fluids*; Safran, S. A., Clark, N. A., Eds.; John Wiley & Sons: New York, 1987; pp 493–507.

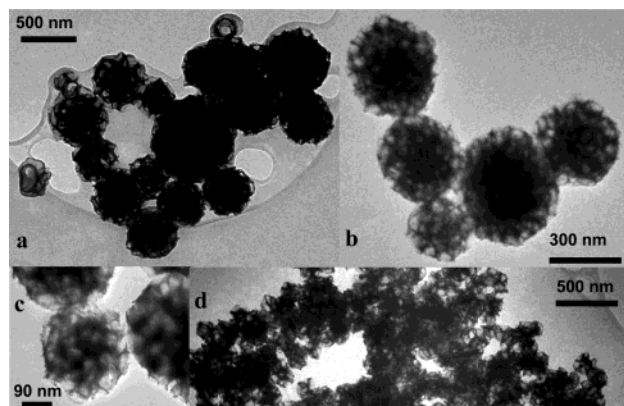


**Figure 2.** Foamlime balls composed of platinum nanosheets and their aggregates.

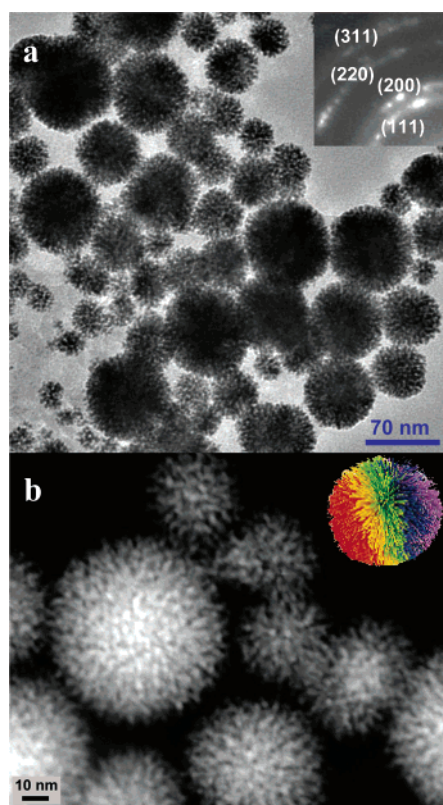


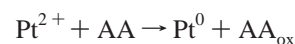
**Figure 3.** (a) TEM image of nanodendrites produced with Brij-35 surfactant in the absence of photocatalyst and (inset) the electron diffraction pattern of a group of the dendrites indicating that they are composed of platinum metal and as a group are polycrystalline. (b) HAADF scanning TEM image of the three-dimensional platinum dendrites grown in the presence of Brij-35 micelles. Inset: a Koosh ball.

The platinum nanostructures obtained in the presence of small surfactant assemblies were further examined using SDS and Brij-35 micelles. Although reduction of the platinum complex proceeds on a time scale similar to that for the circular nanosheets (<30 min), the product obtained has an entirely different morphology (see Figure 3).<sup>44</sup> Bright field TEM images of the reduction product reveal platinum nanostructures that appear to be dendritic but that are now three-dimensional (Figure 3a). The dendritic nature of the nanostructures is more evident in the high-angle annular dark field (HAADF) scanning TEM

images (Figure 3b). As shown by the inset of Figure 3b, the spherical nanodendrites superficially resemble nanoscale versions of common toys called “Koosh balls” (although Koosh balls are not dendritic). All of the reduced platinum found on the TEM grids is in the form of these spherical nanodendrites. It is likely that the nanostructures shown in Figure 3 are three-dimensional analogues of the circular nanosheets shown in Figure 1.

**Mechanism of Nanodendrite Growth and Control of Nanostructure Size.** Key goals in the synthesis of metal nanostructures are that the synthesis gives nanostructures of a specific size and size distribution and that the synthesis is reproducible.<sup>11</sup> To gain control of the synthesis, it was necessary to understand the mechanism by which the nanostructures are formed. A mechanism based on slow, continuous nucleation (seeding) and fast autocatalytic growth has previously been used to explain the growth of metallic nanoparticles.<sup>13</sup> A related mechanism is proposed to explain the formation of the platinum nanodendrites in the present work.

In the seeding/autocatalytic growth mechanism, slow chemical reduction of Pt ions by ascorbic acid occurs to give Pt-nanoparticle growth centers (seeds) at very low concentration by the simplified redox reaction:



When these seeds reach a certain size (~500 atoms), the Pt nanoparticles apparently become autocatalytic for the platinum reduction reaction.<sup>45,46</sup> The seed particles then rapidly grow into the mature nanostructures shown in Figures 1, 2, and 3 as the autocatalytic reduction exhausts the available platinum complex.

For the nanostructures shown in Figure 3, the slow, continuous formation of seed nanoparticles over the entire reaction time leads to a large average size for the nanostructures and a broad size distribution. The latter is due to the variation in the autocatalytic growth period for seed particles produced at different times. Consistent with this mechanism, smaller and more uniform three-dimensional nanostructures are obtained if the micellar reaction solution is initially seeded with ~3 nm Pt nanoparticles prepared by standard methods;<sup>47</sup> these seeds have equal autocatalytic growth times and thus yield small uniform sized nanostructures. So, although the autocatalytic growth is uncontrolled, the size and size distribution of the nanostructures can be controlled by various seeding strategies.

**Photocatalytic Seeding Studies.** An easy, precise, and practicable method for producing a large initial concentration of seeds for controlling the size and uniformity of the nanostructures is to use a photocatalyst and light to rapidly generate the growth centers in situ. This method provides a broad range of possible seed concentrations and rates of formation allowing precise control over the size of the nanostructures. Another potential advantage of the photocatalytic seeding method is that the seed particles, and thus the platinum nanostructure, may be placed at a desired location by pre-positioning the photocatalyst molecules. In the present example, a hydrophobic photocatalyst

(44) Both electron diffraction (inset of Figure 3a) and energy-dispersive X-ray spectra (Figure S2b) of dried samples again confirm that the nanostructures observed are composed of platinum.

(45) In the case of platinum-catalyzed hydrogen evolution, the limiting minimum size for the Pt particle to become catalytic was determined to be as few as 50 atoms, and a stable catalytic particle was created at about 500 atoms. See ref 46.

(46) Greenbaum, E. *J. Phys. Chem.* **1988**, *92*, 4571–4574.

(47) Furlong, D. N.; Launikonis, A.; Sasse, W. H. F.; Sanders, J. V. *J. Chem. Soc., Faraday Trans.* **1984**, *80*, 571–588.

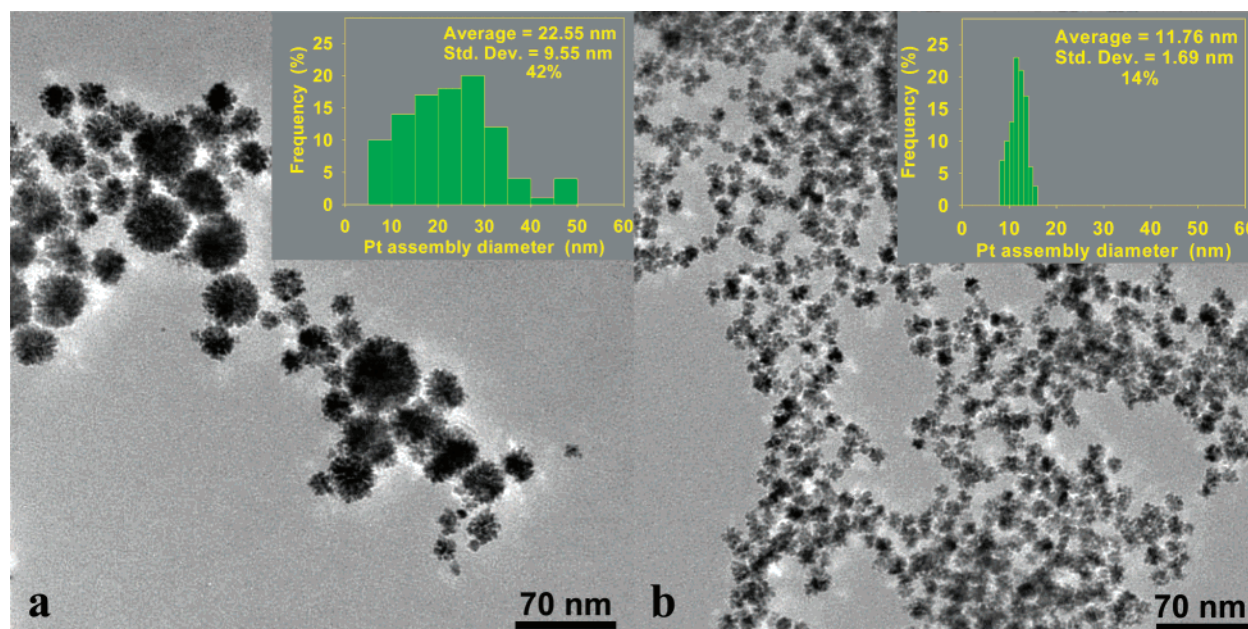
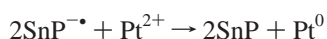
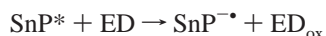
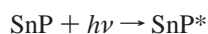


**Figure 4.** TEM images of platinum nanostructures produced in the presence of SDS without (a) and with (b) photocatalyst and their respective size distributions (insets). Average diameters were measured for 100 nanostructures, and their frequencies are plotted in the inset graphs. The average size and the standard deviations are given in the plots, along with the percentage ratio of the standard deviation to average size.

molecule is positioned within the interior of a micelle or within the bilayer of a liposome (as illustrated by the example in Figure 1a) and is used to initiate seed and thus nanostructure growth.

The photocatalyst chosen to generate seeds is a tin(IV)-porphyrin complex (SnP), examples of which are shown in Chart 1. The photocatalytic reduction of platinum salts by the SnP is accomplished in the presence of visible light and an electron donor (ED), ascorbic acid in this case. The SnP photoreaction is a reductive photocatalytic cycle, which has been used previously in the photosynthesis of reduced methyl viologen and to evolve  $H_2$  in the presence of colloidal Pt.<sup>48–50</sup> In the present photoreaction,  $Pt^{2+}$  is reduced as described by the following simplified equations:



Absorption of visible or UV light by the SnP yields the long-lived excited triplet  $\pi-\pi^*$  state,  $SnP^*$ , which is rapidly reduced ( $SnP^*/SnP^{\bullet-}$ , +1.1 V, calculated by adding the triplet state energy to the potential for  $SnP/SnP^{\bullet-}$ ) by an ED such as ascorbic acid. The product is a long-lived<sup>51</sup> radical anion,  $SnP^{\bullet-}$ , which is a strong reductant ( $SnP/SnP^{\bullet-}$ , -0.66 V) capable of efficiently reducing a variety of metal ions including Ag, Au, Hg, Pb, Cu, and Pt to the zerovalent metals.<sup>52</sup> Reduction of the metal regenerates neutral SnP, which again becomes available to absorb light and initiate a successive photochemical cycle. The

photocycle is reductive because the initial electron-transfer event is the reduction of the porphyrin anion by the ED.

To investigate the potential of this photocatalytic seeding method, hydrophobic SnOEP (optical studies suggest the chloride axial ligands are displaced in aqueous solution) was included in an SDS micellar reaction mixture in catalytic amounts ( $\sim 1 \mu M$ ). Although SnOEP is very slightly soluble in water without surfactant, its solubility is much greater in surfactant solutions, indicating that the SnOEP molecules are associated with surfactant assemblies. After exposure to intense incandescent light ( $0.8 \mu mol cm^{-2} s^{-1}$ ) for several minutes, the reaction solution turned black in nearly the same length of time that was observed in the absence of the photocatalyst. However, compared to the nanostructures obtained in the absence of photocatalyst (Figure 4a), the product now consists of small strikingly uniform Pt nanostructures (Figure 4b). To demonstrate that the photocatalytic property of the porphyrin causes the size change rather than the presence of the porphyrin molecule, it was shown that another tin porphyrin, SnT(N-Me-Py)P, had the same effect on nanostructure size as SnOEP. In addition, when the nickel derivative (NiT(N-Me-Py)P), which is photochemically inactive, was substituted in the reaction, it was found to have no effect on the average size or distribution.

Based on TEM images such as those in Figure 4b, Figure S4 of the Supporting Information, and the rotated TEM images shown in Figure 5, the nanostructures generated in the photocatalytically seeded reaction are approximately spherical in shape. Measurements of the nanostructures in the TEM images give an average diameter of  $11.8 \pm 1.7$  nm. Although they appear to consist of joined nanoparticles with particle diameters of  $2.9 \pm 0.1$  nm, a size typical of the particles found in Pt colloids,<sup>47</sup> they are better viewed as “embryonic” dendrites. Additional growth of these nascent dendrites (Figure 4b) would then produce the larger nanostructures seen in Figure 4a.

The insets in Figures 4a and 4b show the respective size distributions obtained from the TEM images. These verify that

(48) Song, X. Z.; Jia, S. L.; Miura, M.; Ma, J. G.; Shelnett, J. A. *J. Photochem. Photobiol.* **1998**, *113*, 233–241.

(49) Shelnett, J. A. *J. Am. Chem. Soc.* **1983**, *105*, 7179–7180.

(50) Kalyanasundaram, K.; Shelnett, J. A.; Gratzel, M. *Inorg. Chem.* **1988**, *27*, 2820–2825.

(51) Under alkaline conditions, the lifetime of the radical anion is approximately 10 s with triethanolamine as the electron donor.

(52) Wang, Z.; Abdelouas, A.; Song, Y.; Gong, W. L.; Lutze, W.; Shelnett, J. A. Manuscript in preparation.

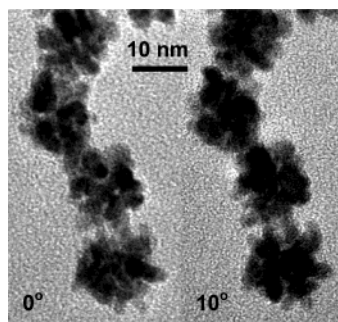


**Figure 5.** Stereoview generated from rotated TEM images of several nanodendrites.

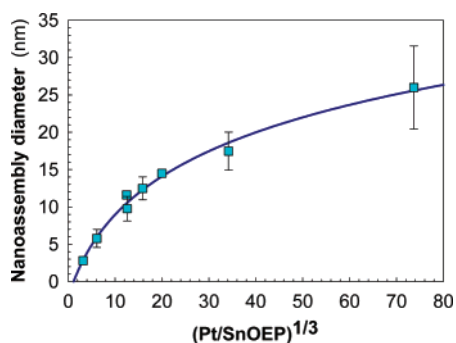


**Figure 6.** Nanostructure diameter versus the cube root of the Pt-to-porphyrin molar ratio (a measure of the nanostructure volume per growth center).

photocatalytic seeding results in a smaller size and a more uniform size distribution. Specifically, when photocatalyst is absent, the standard deviation is 42% of the average size (22.6 nm), indicating a lack of size control. When photocatalyst is present (Figure 4b), the average size is small (11.8 nm) and the standard deviation is only 14% of the average diameter, indicating fair uniformity. Dynamic light scattering confirms that the size difference apparent in the TEM samples in Figure 4 is also present in solution. The diameters measured by light scattering are 14 nm in the presence of photocatalyst and 62 nm in the absence of photocatalyst. The larger sizes found by QELS probably results from some aggregation of the nanostructures in solution.

For this type of growth, the average nanostructure size can be controlled by varying the amount of platinum per initial seed. That is, the autocatalytic reduction will distribute the Pt atoms more or less equally onto the growth centers formed by fast photocatalytic reduction at the beginning of the reaction. One good way to vary the number of seeds is to vary the porphyrin concentration; more porphyrins make more seeds and consequently smaller dendrites at a fixed platinum concentration. Figure 6 shows that the average nanostructure diameter does indeed decrease with increasing porphyrin and thus seed concentration when the total platinum is held constant. Thus, the factor determining the dendrite size in this case is the platinum-to-porphyrin molar ratio. The diameter of the nanodendrites should be related to the cube root of the volume of platinum available for each seed (assuming a spherical structure), which in turn is related to the cube root of the Pt-to-porphyrin molar ratio as shown in Figure 6. Although a linear relationship is not observed, a direct relationship between the two quantities is clearly present.

A straight line is expected in Figure 6 only if the concentration of seeds is directly related to the porphyrin concentration, the principal variable in the data for the plot. Ideally, each porphyrin makes only one seed, and the seed then becomes catalytic and gets its share of the Pt as it grows autocatalytically into the mature nanostructure. The curvature at high SnP concentrations (low ratios) seen in Figure 6 probably results from light-shielding effects, which prevent some porphyrins from getting enough light to generate a seed particle, thus raising the average nanostructure diameter per porphyrin. For the smallest Pt/SnP ratio, individual 3 nm nanoparticles are obtained (first data point). Deviation from linearity in the plot at high ratios is due to competition from the slow seeding by the uncatalyzed chemical reduction, which provides additional seeds and lowers the average diameter. The vertical bars for some of the data points give the standard deviation of the size distribution; the distribution is seen to broaden for low SnP concentrations (large Pt/SnP ratios) because continuous spontaneous seed generation provides some of the growth centers. Note that the graph includes some data points that come from different Pt concentrations, verifying that only the Pt per growth center is important in determining the size.

For the experiments described in Figure 4, the irradiation with intense light continues until the reaction is complete (30 min). However, the photocatalytically generated seeds are produced during the first few minutes because the reaction mixture turns black after this time due to the formation of a concentrated colloid. During this window of opportunity, it is possible to vary the irradiation time to control the number of seeds and thus the size of the nanostructures obtained (Figure 7). In these experiments, the reaction solutions are identical, and intense light exposure ( $800 \text{ nmol cm}^{-2} \text{ s}^{-1}$ ) for the specified times is followed by exposure to ambient room light ( $0.5\text{--}2.0 \text{ nmol cm}^{-2} \text{ s}^{-1}$ ) until the reaction is complete at 30 min total time.

Figure 7 shows that increasing the initial exposure time from 10 to 90 s gives nanostructures with proportionally smaller diameters and narrower size distributions, which is completely consistent with a photocatalytic seeding mechanism. Given that the SnP concentration is the same for all the experiments, the number of growth centers generated is proportional to the exposure time,  $t$ . The Pt concentration is also the same in the reactions ( $\text{Pt/SnP} = 4000$ ), so the diameter of the nanodendrite is related to the cube root of the initial Pt concentration divided by the number of growth centers as discussed above. In other words, the nanostructure diameter is expected to be proportional to the cube root of the initial Pt concentration divided by the exposure time (number of seeds), i.e.,  $([\text{Pt}]_0/t)^{1/3}$ . Obviously this relationship cannot hold for exposure times longer than 3 min (small inverse exposure times), because the reaction mixture turns black and the porphyrins no longer receive light. Similarly, for short exposure times (large inverse exposure times), the size is dominated by the spontaneous formation of seeds by slow chemical reduction. Nonetheless, between these extremes a linear relationship is observed. As expected, for the shortest illumination times, slow spontaneous formation of seeds competes with the photocatalytic process, leading to a broad size distribution (as shown by the “error” bars in the plot in Figure 6). Also as expected, when growth occurs totally in the dark, the average size and size distribution are essentially the same as those seen when no photocatalyst is present.

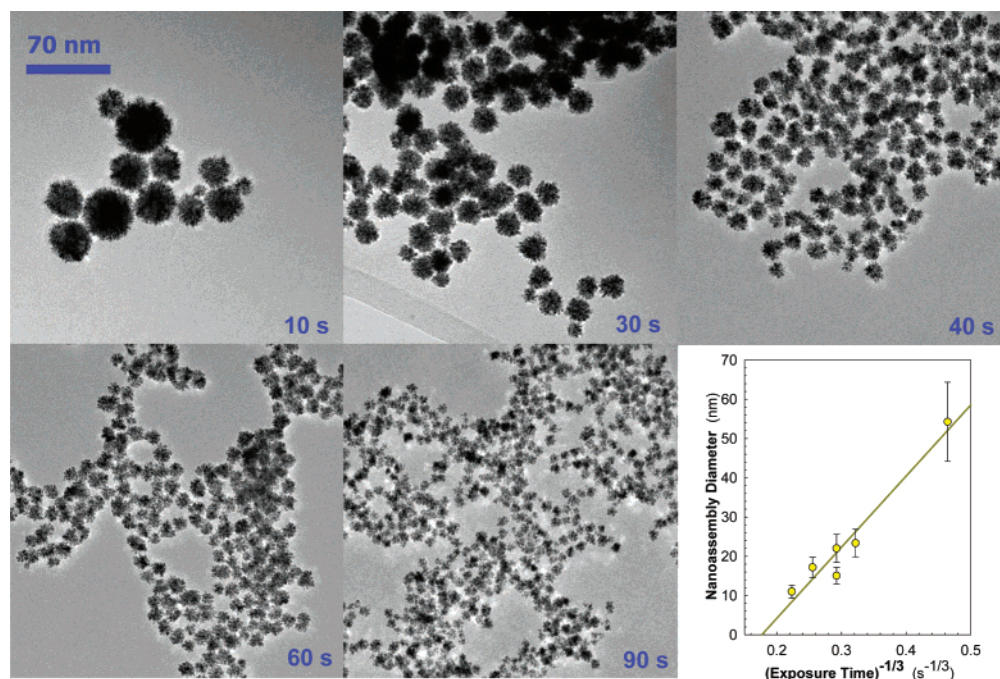


**Figure 7.** TEM images of the nanostructures as a function of intense light exposure time and the relationship between the average diameter of the nanostructures and the cube root of the inverse of the exposure time.

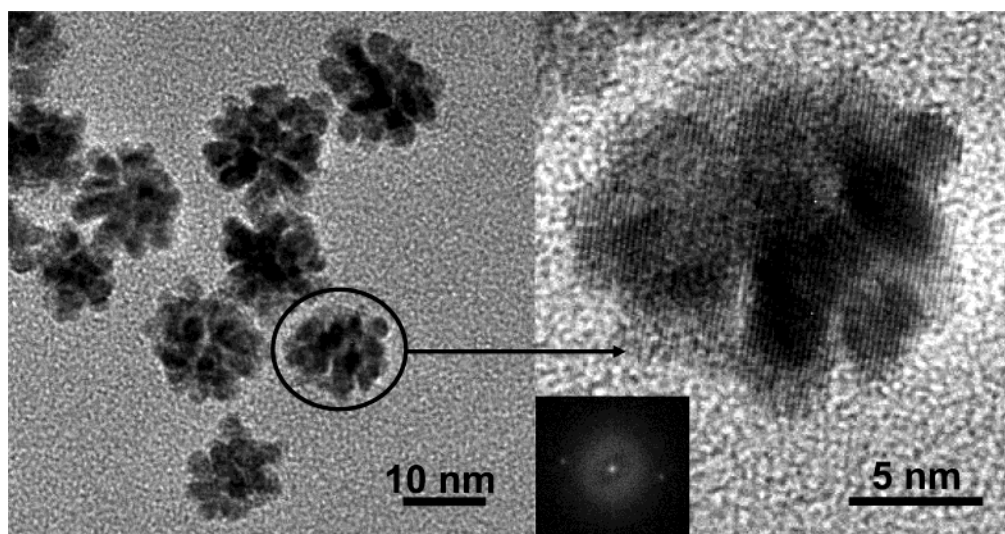


**Figure 8.** TEM image of the small spherical nanodendrites and a high-resolution TEM image of one of them. The nanostructures are produced by fast photocatalytic seeding by the SnOEP and subsequent autocatalytic reduction of  $\text{Pt}^{2+}$  complex by the seed particles. Each nanodendrite is a single crystal, as shown by atomic fringing in the TEM image of one of the nanoassemblies. Inset: selected-area Fourier transform pattern of the high-resolution image of the selected nanostructure. The (111) planes are clearly visible and nearly vertical with a spacing of 0.23 nm.

Porphyrim concentration and light exposure can also be used to control the size and size distribution of the circular nanosheets shown in Figure 1. For example, when SnOEP is included in DSPC liposomes (Figure 1a) even at sub-micromolar concentrations, much smaller and more uniform sized platinum nanosheets are formed (images not shown).

The light-dependent and porphyrin-dependent size control demonstrated in this work explicitly confirms the seeding and autocatalytic growth mechanism put forward to explain the uncontrolled growth of the nanostructures obtained when photocatalyst is not present (Figures 1, 2, and 3). It also rules out alternative mechanisms for formation of the nanostructures such as those based on nanoparticle aggregation.

A more detailed examination of the small nanostructures shown in Figures 4b revealed crystallographic alignment of the individual nanoparticles (Figures 8), making the entire nanostructure one single crystal as expected for dendritic growth. The crystallinity of the nanodendrites is demonstrated by the Fourier transform (inset) of the atomic lattice fringing apparent in the image. Additional evidence for the crystallinity of the nanostructures is provided in Figure 9, which shows the TEM image of a group of the small nanodendrites and the indexed convergent beam electron diffraction patterns of seven of the nanodendrites in the image. These results verify that most of these three-dimensional nanodendrites are indeed single crystals, as was the case for

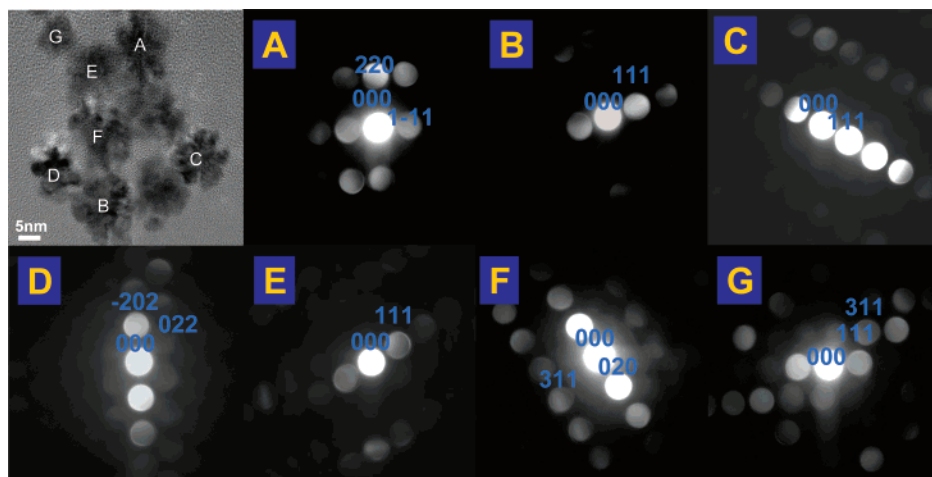


**Figure 9.** High-resolution TEM image showing several labeled nanodendrites and their convergent beam electron diffraction patterns. The electron diffraction patterns verify that the nanostructures are single crystals and that each nanodendrite has a different orientation on the TEM grid. The indexing gives the different crystallographic orientations of the individual nanostructures.

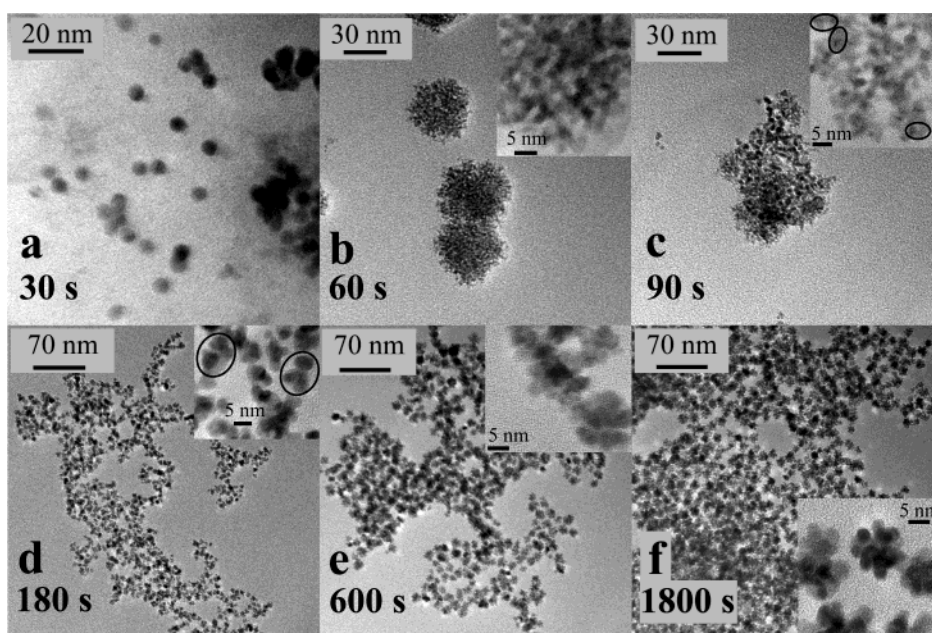


**Figure 10.** TEM images showing the time development of the small nanodendrites. (a) Pt seed particles are formed during the first 30 s under intense illumination; (b) at 60 s, more seed particles are observed in loose groupings associated with surfactant; (c) at 90 s, the seeds have grown a crystallographically aligned bud or branch (indicated by ellipses), a process that breaks up the seed groupings; (d) by 3 min, the seeds have grown several aligned buds (ellipses) and the seed groupings have mostly broken up; (e) at 10 min, the nanostructures are almost fully developed; (f) growth is complete at 30 min.

the two-dimensional nanosheets shown in Figure 1 (see also Figure S3).

To our knowledge, this is the first example of this type of single-crystalline metallic nanodendrite. Consistent with their single-crystalline structure, the nanodendrites are stable in solution for at least three months. Even after taking the colloidal suspension to dryness and resuspending the solid by mild sonication in the same solvent system, TEM images show that the structures of these nanodendrites are essentially unchanged.

**Morphological Evolution of the Nanodendrites.** To develop a more complete understanding of the seeding and dendritic growth processes, TEM samples obtained using SDS micelles were prepared at specific times during exposure to intense incandescent light. Washing and drying during the TEM sample preparation process effectively interrupts the reduction reaction, giving a snapshot of the nanostructures present at the time the sample is prepared. The TEM images of these samples are

shown in Figure 10. This time-development study reveals the stages in the development of mature nanostructures such as those in Figure 8. At 30 s of illumination, individual particles are observed with diameters of about 6 nm suggestive of a thin spherical shell of platinum coating the micelle. The structures are unstable under the intense electron beam and pop open, forming several fragments. By 60 s, the Pt in these 6 nm shells apparently redistributes since we now observe only 3–4 nm particles that tend to aggregate with surfactant into randomly oriented groupings, forming a ragged disk. This structure is likely an artifact of drying with surfactant present during the sample preparation. By an illumination time of 90 s, the original seed particles have begun to grow crystallographically aligned buds (branches), and the aggregates of seeds have partially broken up as a consequence. At 3 min, the initial seed particles have sprouted several additional crystallographically aligned buds, and formation of these immature nanostructures has largely

broken up the seed aggregates. By 10 min, the growing nanostructures contain most of their full complement of branches, and at 30 min and 1 h, the mature nanostructures are observed. TEM images of Pt nanoparticles obtained by Troupis et al.<sup>53</sup> using polyoxometalate photocatalysts (e.g., [SiW<sub>12</sub>O<sub>40</sub>]<sub>4</sub>) and UV light are in clusters that could be similar to either the seed clusters in Figure 10b or the nanoassemblies in Figure 10f, but the TEM images reported are not of sufficiently high resolution to allow us to distinguish between these two possibilities.

The 6 nm shell-like structures seen at the earliest times suggest that the SDS micelles might actually serve a templating role as is the case of the liposomes for the circular nanosheets (Figure 1). Indeed, scanning TEM HAADF images of the mature photocatalytically seeded nanodendrites do show that many of them have *z*-density profiles with a dip in the center (see Figure S4). This result is consistent with these nanostructures lacking a metallic interior and possibly containing a surfactant micelle. We note, however, that seeding with Pt nanoparticles as opposed to using a photocatalyst molecule in the micelle produces essentially indistinguishable nanodendrites. This does not rule out a templating role for the micelles, as the added nanoparticle might attach itself to the surface of a micelle, and then branching during the autocatalytic growth phase could then ultimately coat the micelle to produce the observed nanostructure. Alternatively, the nanoparticles may simply accrete a layer of surfactant and grow into the nanodendrite without the micelles, providing a templating function. In this regard, it is worth noting that the nanostructures formed at surfactant concentrations (1 mM) well below the critical micellar concentration (CMC) of SDS (~8 mM) are identical to those formed at concentrations above the CMC. However, because of the marked (50- to 200-fold) decrease in the CMC in the presence of porphyrins,<sup>54</sup> micelles likely still exist to act as templates. Even where a templating role seems to be readily apparent (e.g., as for the liposomes in Figure 1) it is not always clear how this effect occurs. For example, the sheets could be formed on the surface, in the bilayer, or between liposomes. In summary, these results suggest that although surfactant must be present to form these nanostructures, the surfactant need not necessarily play a templating role.

The surfactant is almost certainly involved in interfacially directing the dendritic growth of the three-dimensional nanostructures. Above the CMC, the metal surface of the growing Pt dendrite most likely becomes fully coated with a bilayer of surfactant.<sup>55</sup> The oxidation of ascorbic acid and addition of platinum metal to the growing dendrite can then occur at the metal surface beneath this protective surfactant bilayer. Accretion of additional surfactant from solution onto the growing platinum surface protects the embryonic nanostructure. Below the CMC, there is not enough surfactant to form a bilayer,<sup>55</sup> but most likely the platinum surface is still covered with surfactant molecules. The fact that nanodendrites form even below the CMC may indicate that the exact molecular structure of the surfactant layer is not critical for directing dendritic

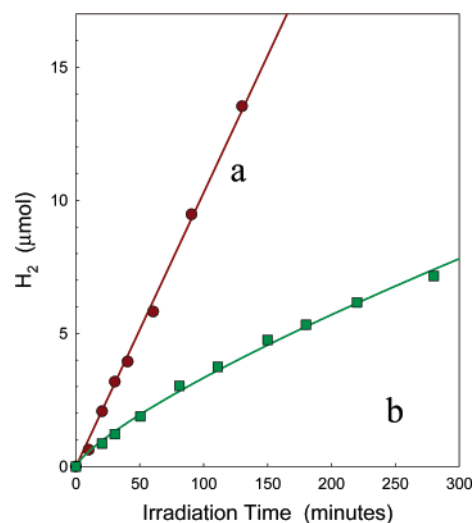


**Figure 11.** Photocatalytic reduction of water to hydrogen by the platinum nanostructures, composed of the platinum nanodendrite, surfactant, and SnOEP, with SnUroP (80 mM) added to improve light harvesting. The Pt nanostructures are diluted into an ascorbic acid (ED) solution containing the Sn uroporphyrin for the measurement. Water is reduced at rates as high as 6 mmol h<sup>-1</sup> (H<sub>2</sub> turnover rate of 33 h<sup>-1</sup> in terms of SnUroP) by electrons supplied to the surface of the Pt catalyst primarily by the light-harvesting Sn uroporphyrin anions. Incandescent white light intensity is 800 nmol cm<sup>-2</sup> s<sup>-1</sup>, but mostly light with wavelengths in the region of the Soret band of the porphyrin is absorbed. Reaction conditions are (a) low Pt (6.5 mM) and high ascorbic acid concentration (200 mM) and (b) high Pt concentration (65 mM) with low ascorbic acid concentration (60 mM). H<sub>2</sub> turnover rates in terms of atomic Pt are (a) 390 h<sup>-1</sup> and (b) 14 h<sup>-1</sup>.

growth; this is consistent with the fact that surfactants with both negative (SDS) and neutral (Brij-35) headgroups (Chart 1) are equally capable of producing the three-dimensional nanostructures. It is also possible that ascorbic acid or its oxidation product may play some role in interfacially directing the dendritic growth. The importance of the interfacially directed growth process is supported by experiments in which pyridine, which interacts strongly with the platinum surface, is added to the Brij-35 reaction mixture in small amounts. In this case, nanoparticles instead of the three-dimensional nanodendrites are formed, consistent with pyridine effectively interrupting the interfacial interactions of platinum with the surfactant.

A reasonable mechanism by which the surfactant layer might give dendritic growth is by controlling the diffusion of reactants to the platinum surface. Most likely, diffusion of Pt complex and ascorbic acid into the approximately 1 nm wide surfactant-filled crevices between the arms of the three-dimensional dendrites is slower than the diffusion to the nanostructure extremities. This differential diffusion rate results in dendritic growth in a “rich gets richer” scenario. Note that at pH 3 ascorbic acid is fully protonated and neutral so it can easily diffuse through the surfactant layer. Similarly, the predominant Pt(Cl)<sub>2</sub>(H<sub>2</sub>O)<sub>2</sub> complex is also neutral and can easily diffuse across neutral and charged surfactant layers. In the case of the two-dimensional dendrites, diffusion may be limited by the sheet being sandwiched between two liposomes, so that nutrients can only diffuse to the edge of the nanosheet.

Regardless of the exact organization of the metal and surfactant molecules, the photocatalytically active porphyrin molecule likely remains associated with surfactant in the nanostructure that it nucleated. As colloidal platinum is a well-known catalyst for H<sub>2</sub> evolution from water in artificial

(53) Troupis, A.; Hiskia, A.; Papaconstantinou, E. *Angew. Chem., Int. Ed.* **2002**, *41*, 1911–1914.

(54) Savitski, A. P.; Vorobyova, E. V.; Berezin, I. V.; Ugarova, N. N. *J. Colloid Interface Sci.* **1981**, *84*, 175–181.

(55) Mafuné, F.; Kohno, J.; Takeda, Y.; Kondow, T.; Sawabe, H. *J. Phys. Chem. B* **2000**, *104*, 8333–8337.

photosynthesis systems,<sup>56–60</sup> the Pt nanostructure and the associated porphyrin photocatalyst should therefore be able to generate H<sub>2</sub> in the presence of light and an electron donor. This H<sub>2</sub> photosynthetic chemistry is similar to the reaction mechanism described above for Pt<sup>2+</sup> reduction, except that SnP<sup>•-</sup> provides electrons to H<sup>+</sup> at the Pt metal surface to produce hydrogen. To see if hydrogen evolution was occurring, the reaction mixture containing the (12 nm) three-dimensional platinum dendrites and associated porphyrin photocatalyst (as shown in Figure 8) was irradiated with room light in the presence of ascorbic acid. After two months, the headspace of the sealed reaction vessel was analyzed by gas chromatography, and the presence of hydrogen was confirmed (~30 vol %). Two interesting aspects of this catalytic reaction are that H<sub>2</sub> evolution is observed even in the presence of the surfactant coating and that the porphyrin delivers its strongly reducing electrons directly to protons at the Pt surface without the aid of a relay molecule such as methyl viologen, as has been used in some previous studies.<sup>56</sup>

The nanodendrite–surfactant assemblies probably suffer from poor light-harvesting ability because of the low concentration of the light-absorbing porphyrin per nanodendrite and the opacity of the colloidal solution. To address these deficiencies, water-soluble SnUroP (Chart 1) was added to an ascorbic acid solution containing only a small amount of the nanodendrite mixture. In this case, H<sub>2</sub> evolution is greatly accelerated, consistent with increased light flux and the additional light harvesting provided by the SnUroP. (Dilution of the nanodendrites may have also altered the surfactant coating and accelerated H<sub>2</sub> evolution.) As shown in Figure 11, hydrogen evolution increases linearly for hours with turnover rates as high as 390 h<sup>-1</sup> (mole H<sub>2</sub>/mole atomic Pt). Given these findings, nanostructures such as those seen in Figure 8 can be viewed as functional nanocomposites consisting of the platinum dendrite, the adsorbed surfactant, and possibly ascorbic acid, and the associated active photocatalyst.

## Conclusions

The results reported here demonstrate that seeding and autocatalytic growth by reduction of Pt salts in the presence of surfactants leads to unique two- and three-dimensional platinum nanodendrites. The platinum dendrites are formed by interfacially directed growth and restricted access of nutrients due to the surfactant on the surface of the growing nanostructure. In the case of large liposomes, templating by the surfactant results

in sheetlike nanodendrites or foamlike nanosheets of platinum. The unique surfactant-templated platinum growth demonstrated by these two-dimensional dendrites presents the possibility of making other new metal nanostructures using different surfactant phases and other materials as templates. Such porous platinum nanomaterials prepared by this method have potential applications in catalysis, electronics, sensors, and magnetic devices.

A novel photocatalytic seeding approach provides a new in situ method of varying the concentration of seeds and thus the final size of the nanostructures. This method presents new opportunities for controlling seeding rates by varying photocatalyst concentration and light intensity. Importantly, it also offers the potential for controlling the synthesis of platinum nanostructures by lithographic techniques, i.e., controlling the location at which nanostructures are grown. Besides lithographic control, the location might also be controlled by pre-positioning and immobilizing the photocatalyst molecules in a desired pattern. For the 3-D nanodendrites, the particular micelles that contain a porphyrin molecule are those that lead to growth centers. For the 2-D nanodendrites, the location at which growth occurs is probably determined by the location of the porphyrin photocatalyst in the templating surfactant as illustrated in Figure 1a.

**Acknowledgment.** We thank Daniel Throckmorton for preparing liposomes. This work was partially supported by the Division of Materials Sciences and Engineering, Office of Basic Energy Sciences, U.S. Department of Energy, by the Division of Chemical Sciences, Geosciences and Biosciences, Office of Basic Energy Sciences, U.S. Department of Energy (DE-FG02-02ER15369), the Laboratory Directed Research and Development Program at Sandia National Laboratories, and the Luso-American Development Foundation (FLAD) Nanotechnology Network (to E.P. and J.A.S.). Sandia is a multiprogram laboratory operated by Sandia Corporation, a Lockheed Martin Company, for the United States Department of Energy's National Nuclear Security Administration under Contract DE-AC04-94AL85000.

**Supporting Information Available:** Figures showing UV–visible spectra demonstrating the degradation of ascorbic acid in air and the acceleration of this reaction in the presence of platinum nanoparticles; electron-dispersive X-ray spectra of 2-D and 3-D nanodendrites; high-resolution TEM images of a circular nanosheet; and HAADF scanning TEM image of small 3-D nanodendrites and density profiles for six randomly selected dendrites (PDF). This material is available free of charge via the Internet at <http://pubs.acs.org>.

JA037474T

(56) Krüger, W.; Fuhrhop, J.-H. *Angew. Chem., Int. Ed. Engl.* **1982**, *21*, 131.

(57) Kalyanasundaram, K.; Grätzel, M. *Helv. Chim. Acta* **1980**, *63*, 478–485.

(58) Pileni, M.-P.; Braun, A. M.; Grätzel, M. *Photochem. Photobiol.* **1980**, *31*, 423–427.

(59) Mercer-Smith, J. A.; Mauzerall, D. *Photochem. Photobiol.* **1981**, *34*, 407–410.

(60) McLendon, G.; Miller, D. S. *J. Chem. Soc., Chem. Commun.* **1980**, 533–534.